The Course of Tissue Permeabilization Studied on a Mathematical Model of a Subcutaneous Tumor in Small Animals

Nataša Pavšelj, Zvonko Bregar, David Cukjati, Danute Batiuskaite, Lluis M. Mir, and Damijan Miklavčič*

***Abstract*—One of the ways to potentiate antitumor effectiveness of chemotherapeutic drugs is by local application of short intense electric pulses. This causes an increase of the cell membrane permeability and is called electropermeabilization. In order to study the course of tissue permeabilization of a subcutaneous tumor in small animals, a mathematical model was built with the commercial program EMAS, which uses the finite element method. The model is based on the tissue specific conductivity values found in literature, experimentally determined electric field threshold values of reversible and irreversible tissue permeabilization, and conductivity changes in the tissues. The results obtained with the model were then compared to experimental results from the treatment of subcutaneous tumors in mice and a good agreement was obtained. Our results and the reversible and irreversible thresholds used coincide well with the effectiveness of the electrochemotherapy in real tumors where experiments show antitumor effectiveness for amplitudes higher than 900 V/cm ratio and pronounced antitumor effects at 1300 V/cm ratio.**

***Index Terms*—Electropermeabilization, electroporation, finite element modeling, subcutaneous tumor model, tissue conductivity change.**

I. Introduction

THE application of electric pulses to cells, either in suspension or in tissue, causes structural changes in the cell membrane, which becomes more permeable [1]–[4]. If pulse amplitude, duration and number of pulses are correctly set, the change in the membrane permeability facilitates the cell uptake of ions, molecules such as DNA or drugs, which otherwise can not cross the membrane. Electropermeabilization is used in gene transfection, electrochemotherapy and transdermal drug delivery. The cell membrane is permeabilized when a threshold transmembrane voltage is reached, i.e., when the external electric field is above the reversible threshold value. Unfortunately the portion of the cells that suffers permanent damage is increased by increasing the electric field, so when the electric field reaches an irreversible threshold value, the electropermeabilization becomes irreversible and causes cell death. In the case of electrochemotherapy, exceeding the irreversible threshold in tumor is less problematic, since killing tumor cells is the aim of the treatment, while in electrogenetransfer the electroporation should not damage the electroporated cells. Therefore, the goal is to apply an electric field that will be between the reversible and irreversible permeabilization thresholds [5].

Electropermeabilization of cells depends on the cell and tissue parameters (tissue specific conductivity, cell size, shape, and distribution [6]–[8]), pulse parameters (pulse duration, amplitude, and number of pulses [9]), and the most important parameter, the electric field strength, which causes a transmembrane voltage change on the cell membrane [10]. The specific conductivity of the tissue increases when permeabilized, which could be used as an indicator of the level of the electropermeabilization in the tissue in question [11], [12].

To use electroporation in clinical applications effectively, we have to detect if the target tissue area is permeabilized or not. This feedback could then be used to adjust the electroporation parameters during the treatment to make it more efficient. A theoretical study was performed to monitor the process by means of electrical impedance tomography imaging [12]. Studying the electric field distribution in the biological systems is a relatively simple and useful method to get an insight into some biological processes [13]–[15]. Experimenting on mathematical models is easier and more ethical than performing *in vivo* experiments. We can easily change the excitation of the model by simply applying different boundary conditions. A good mathematical model, verified by experimental data gives us a good insight into the process, but we have to be aware of its limitations. A mathematical model is only an approximation of a very complicated real system and it can not be a substitute for all *in vivo* experimental work. However, it helps us as a source of extra information and helps us to plan future *in vivo* experiments.

Monitoring cell or tissue permeabilization in real time has been of interest for many researchers [12], [16], [17]. In our study, we built a mathematical model of a subcutaneous tumor in small animals and with the help of the model studied the electroporation process during the electrochemotherapy taking into account the increase in tissue conductivity due to cell membrane electroporation. Namely, when the electric field exceeds

Manuscript received September 22, 2004; revised January 9, 2005. This work was supported in part by the European Commission under the 5th framework under Grant Cliniporator QLK-1999-00484 and in part by the Ministry of Science, Education and Sports of the Republic of Slovenia. *Asterisk indicates corresponding author*.

N. Pavšelj and D. Cukjati are with the Faculty of Electrical Engineering, University of Ljubljana, Ljubljana 1000, Slovenia (e-mail: natasa@lbk.fe.uni-lj.si; david@lbk.fe.uni-lj.si).

Z. Bregar was with the Faculty of Electrical Engineering, University of Ljubljana, 1000 Ljubljana, Slovenia. He is now with Milan Vidmar Electroinstitute, 1000 Ljubljana, Slovenia (e-mail: zvonko.bregar@eimv.si).

D. Bautiskaite was with the UMR 8121 CNRS, Institute Gustave-Roussy, Villejuif, France. She is now with the Department of Biology, Vytautas Magnus University, 44248 Kaunas, Lithuania (e-mail: a8daba@vaidila.vdu.lt).

L. M. Mir is with the UMR 8121 CNRS, Institute Gustave-Roussy, 94805 Villejuif, France (e-mail: luismir@igr.fr).

*D. Miklavčič is with the Faculty of Electrical Engineering, University of Ljubljana, 1000 Ljubljana, Slovenia (e-mail: damijan@lbk.fe.uni-lj.si).

Digital Object Identifier 10.1109/TBME.2005.851524

the reversible threshold, the tissue conductivity increases. This change subsequently causes the change of the electric field distribution and of the corresponding current. This process continues until the magnitude of the electric field nowhere in the model exceeds the reversible threshold value or the specific conductivity was already changed in that part of the tissue. We modeled the dynamics of the electroporation process with a sequence of static models that describe electric field distribution at discrete time steps during the process. This is another attempt to describe change of specific conductivity (σ) during electroporation *in vivo* as a process and to determine the ratio (σ_1/σ_0) between the specific conductivity of the electroporated tissue (σ_1) and the specific conductivity of the same tissue before the pulses are applied (σ_0) [18]–[21]. We tuned the model to the experimental data that are also reported, on different separate tissues and compared it with the experimental data on subcutaneous tumors with plate electrodes pressed against the skin.

II. Materials and Methods

A. Finite-Element Method

Electric field and reaction current calculations were made by means of the commercial program EMAS [22] (Ansoft, Pittsburgh, PA) based on finite element method [23]. This method solves partial differential equations by dividing the model into small elements where the quantity to be determined is approximated with a function or is assumed to be constant throughout the element. Finite elements can be of different shapes and sizes, which allows modeling of intricate geometries. Nonhomogeneities and anisotropies can also be modeled and different excitations and boundary conditions can be easily applied. Building a mesh is an important part of the modeling process. One has to be aware where in the model to expect higher gradients of the quantities to be determined. The mesh has to be denser there for the calculation to be exact. Therefore, the mesh has to be denser around the electrodes and on the border between the regions of very different specific conductivities. One of the basic verifications of the model is making a denser mesh to see if it has any effect on the results. If not, the mesh density is adequate. Using the symmetry of the geometry [24], models can also be simplified by applying appropriate boundary conditions.

B. In Vivo Experiments and Measurements

The study is based on the data collected during an extensive study of the response of different tissues to high voltage pulses. The pulses were delivered through plate electrodes to rat skeletal muscle, skinfold, and mouse tumors. Plate electrodes consisted of two parallel metal plates, separated by 5.7 mm for rat's skeletal muscles (the triceps brachii muscle of the hind limb and the gastrocnemius medialis muscle of the forelimb), 5.2 mm for mouse tumors and by 2.8 mm for skinfold. Good contact between the electrodes and tissue was assured by the use of a conductive gel (EKO-GEL, Camina, ultrasound transmission gel, Egna, Italy). The plate electrodes were placed directly to the skeletal muscle and tumor as presented in Fig. 1(a) and Fig. 3(a), respectively. For the electroporation protocol a train of 8 square-wave pulses of 100 μs duration, delivered at a repetition frequency of 1 Hz and generated by a PS 15 electropulsator

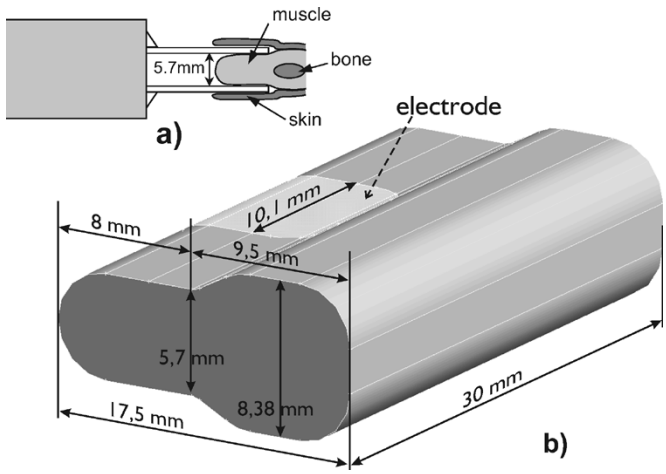

Fig. 1. (a) Geometry of the measurement setup. (b) Model made in EMAS for rat muscle without skin.

(Jouan, St. Herblain, France) was used in all experiments. One experiment per rat extremity (38 muscles) and one per tumor (45 melanomas B16, 46 LPB sarcomas) was performed. Female C57Bl/6 mice purchased from Janvier (France) were used for experiments. They were maintained at 22 °C with a natural day/night light cycle in a conventional animal colony, fed, and watered ad libitum. Subcutaneous tumors were implanted by injecting viable syngeneic LPB sarcoma cells under the skin on the mice flanks of 8–12 wk old mice. The animals were used after 10 to 12 d, when tumors reached at least 5.2 mm in diameter. In addition 12 experiments were performed on rat skinfold.

During the electric pulse the actual current delivered and the applied voltage were acquired by digital oscilloscope. Furthermore, we determined tissue cell permeabilization level by means of the quantitative $^{51}\mathrm{Cr}-\mathrm{EDTA}$ uptake method [25]. Briefly, animals were anesthetized by means of the intraperitoneal administration of the anesthetics Ketamine (100 mg/kg; Ketalar, Panpharma, France) and Xylazine (10 mg/kg; Rompun, Bayer, France). Then rats were given 200 μl and mice 100 μl of $^{51}\mathrm{Cr}-\mathrm{EDTA}$ (Amersham, U.K.) with a specific activity of 3.7 MBq/ml, by an intravenous injection, 5 min before the delivery of the electric pulses. The injected $^{51}\mathrm{Cr}-\mathrm{EDTA}$ distributes freely in the vascular and extracellular compartments, but does not enter the intracellular compartments unless access is provided, e.g., by electroporation. Animals were sacrificed 24 hours after $^{51}\mathrm{Cr}-\mathrm{EDTA}$ injection and tissues exposed to electric pulses were taken out, weighed and counted in a Cobra 5002 gammacounter (Packard Instrument, Meridien, CT). The net $^{51}\mathrm{Cr}-\mathrm{EDTA}$ uptake as a result of elecroporation was calculated as the measured activity per gram of the tissue exposed to the electric pulses. The measured activity could then be converted to the corresponding nanomoles of $^{51}\mathrm{Cr}-\mathrm{EDTA}$ internalized per gram of tissue as a result of tissue cell electroporation.

III. Numerical Models

A. Single Tissue Models

First we modeled the *in vivo* experimental tissue-electrode setups of each tissue separately: muscle, skinfold, and tumor. We modeled the electroporation process in each tissue separately and compared the results of the model with the measured

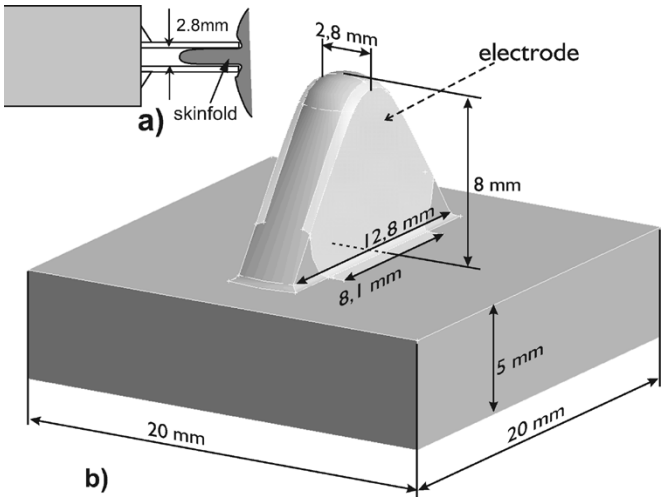

Fig. 2. (a) Geometry of the measurement setup. (b) Model made in EMAS for rat skinfold.

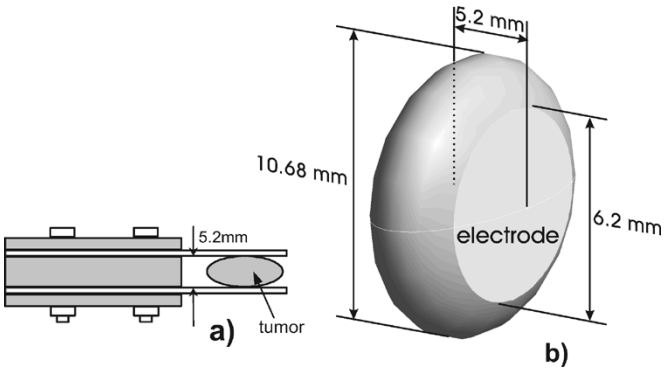

Fig. 3. (a) Geometry of the measurement setup. (b) Model made in EMAS for mouse tumor without skin.

data. We fine tuned the electroporation parameters of the single tissue models, such as initial specific conductivities, electropermeabilization thresholds, changes in specific conductivity and the function describing the specific conductivity dependence $(\sigma(\mathrm{E}))$ between the reversible and the irreversible thresholds, until we established good agreement between the output of the model and the experimental data.

The geometries of measurement setups for the muscle, skin and tumor are presented in Fig. 1(a), Fig. 2(a), and Fig. 3(a) and the corresponding models in EMAS are described in Fig. 1(b), Fig. 2(b), and Fig. 3(b).

In the EMAS models the electrodes were not modeled as a physical element but as boundary conditions. In this way the number of elements in the model was reduced without affecting the results. The presence of the conductive gel between the electrodes and the tissue was also modeled in similar manner, i.e., the area of contact between the tissue and the electrodes is larger, thus the boundary condition is applied to the area beyond the boundaries of the electrode dimensions, typically 0.5 mm on each side. In the muscle model the bone was not considered since its conductivity is low and the bone in the experiments was rather distant from the electrodes. Nor were in the skinfold model modeled different layers of skin. Instead the tissue was considered as homogeneous throughout the model. Namely, large differences in thickness between different layers would unnecessarily complicate the model to the extent where numerical

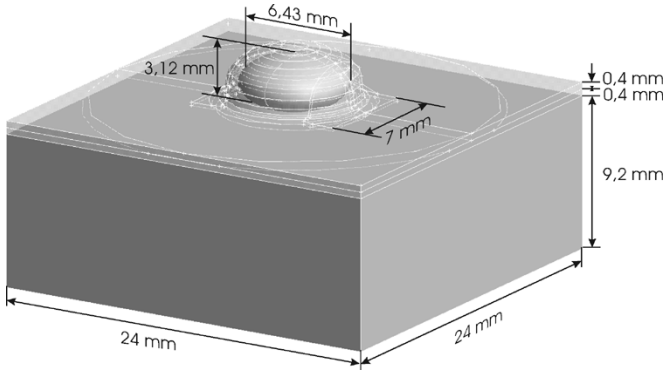

Fig. 4. Model made in EMAS for subcutaneous tumor.

problems could make the calculation impossible. The skin itself was not the primary target of investigation; therefore, an average specific conductivity was assigned to the skin tissue.

B. Intricate Subcutaneous Tumor Model

After setting the threshold values, conductivity changes and the conductivity dependence function between the thresholds for each tissue separately in single tissue models, we built an intricate subcutaneous tumor model. The electric pulses were applied on the skin with plate electrodes pressed against the skin. The model is composed of four different tissues: skin, connective tissue, tumor, and muscle. Underlying tissues such as the bone were not modeled since the field is limited to the tissues lying closer to skin. In Fig. 4, the geometry of the tumor model is presented. The electrodes were again modeled as a boundary condition, not as a physical element, and the boundary condition was extended for 0.5 mm to each side of the electrode to account for the presence of the conductive gel. The distance between electrodes is 8 mm. We later compared the results with measurements done on subcutaneous tumors where the same electrode distance was used.

C. The Electroporation Process

To model the electric field distribution in the tissue-electrode setups, the numerical values of tissue dielectric properties, such as specific conductivity and permittivity were needed. A literature survey of dielectric properties of the biological tissues used here was carried out [26]–[45].

In the model, only the specific conductivity data were used. Namely, direct current analysis was performed, so different permittivity values of the tissues do not play any role in the electric field distribution. When voltage is applied to the electrodes, the electric field is distributed in the tissue according to geometry and specific conductivity ratios of the tissues in the model.

During the analysis, tissue specific conductivities had to be changed according to the level of the tissue electropermeabilization. However, in EMAS we cannot dynamically change material properties, such as specific conductivity. Therefore, we developed a subprogram that uses input and output files of the program EMAS to simulate the electroporation process in discrete steps. Time intervals between steps are, in general, not uniform. Different steps represent stages of specific conductivity changes in tissue and do not have a time value associated with them. They do, however, follow a chronological order starting at step

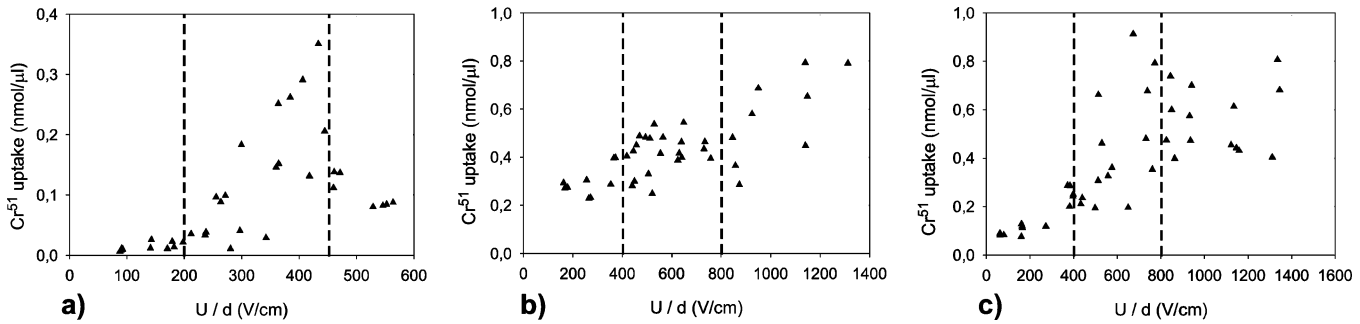

Fig. 5. $^{51}\mathrm{Cr}-\mathrm{EDTA}$ uptake values with respect to the applied voltage for (a) muscle (electrode distance: 5.7 cm). (b) Tumor melanoma B16 (electrode distance: 5.2 cm). (c) Tumor LPB sarcoma (electrode distance: 5.2 cm).

0 and ending at step 5 when the process of electroporation is considered to be completed. Also, it needs to be emphasized that thenumber of iterations is not equivalent to the number of pulses. The whole process is considered to be completed during the first pulse and well inside the first 100 μs. At the beginning of the process, the electric field distribution in the model is computed using EMAS, then after the analysis the subprogram searches in the output file the elements where the electric field exceeds the reversible electropermeabilization threshold. In the second step, the specific conductivities of those elements are changed according to the preset parameters of the electroporation process. Thus the quasi-dynamic model consists of a sequence of static models where according to electric field intensities from the preceding time discrete step, tissue conductivity is changed in the next step. The process is repeated until the electric field distribution reaches its steady state. The steady state occurs when two conditions are met: 1) there are no more elements in the model where the magnitude of the electric field exceeds the reversible threshold value and 2) the specific conductivity was already changed in the elements in which the threshold was reached and exceeded. The process of electroporation is then considered to be completed.

The sequential analysis is performed automatically; the user needs to provide an input file with all the data of the model and a file with all the electroporation parameters, such as the electric field threshold values for reversible and irreversible electropermeabilization, the change in conductivity and the function describing the specific conductivity dependence on the electric field between the reversible and irreversible thresholds. The subprogram that was developed gives us a choice of five different conductivity dependence Step 1) ($\sigma(\mathrm{E})$) functions; 2) linear function; 3) and 4) two exponential function-based dependences; and 5) a sigmoid

$$\sigma(\mathrm{E}) = \begin{cases} \sigma_0 & \mathrm{E} < \mathrm{E}_0 \\ \sigma_1 & \mathrm{E} \geq \mathrm{E}_0 \end{cases} \tag{1}$$

$$\sigma(\mathrm{E}) = \frac{\sigma_1 - \sigma_0}{\mathrm{E}_1 - \mathrm{E}_0} \cdot \mathrm{E} + \sigma_0 \tag{2}$$

$$\sigma(\mathrm{E}) = \mathrm{A}\left(1 - \mathrm{e}^{\frac{\mathrm{E}-\mathrm{E}_0}{\mathrm{B}}}\right) + \sigma_0$$

where

$$\mathrm{A} = \frac{(\sigma_1 - \sigma_0)}{\left(1 - \mathrm{e}^{\frac{\mathrm{E}_0-\mathrm{E}_1}{\mathrm{B}}}\right)} \tag{3}$$

$$\sigma(\mathrm{E}) = \mathrm{A}\left(\mathrm{e}^{\frac{\mathrm{E}-\mathrm{E}_1}{\mathrm{B}}} - 1\right) + \sigma_1$$

where

$$\mathrm{A} = \frac{(\sigma_0 - \sigma_1)}{\left(\mathrm{e}^{\frac{\mathrm{E}_0-\mathrm{E}_1}{\mathrm{B}}} - 1\right)} \tag{4}$$

$$\sigma(\mathrm{E}) = \sigma_0 + \frac{(\sigma_1 - \sigma_0)}{\left(1 + \mathrm{e}^{\frac{\mathrm{A}-\mathrm{E}}{\mathrm{B}}}\right)}$$

where

$$\mathrm{A} = \frac{\mathrm{E}_0 + \mathrm{E}_1}{2}. \tag{5}$$

Symbols σ_0 and σ_1 in (1) to (5) are the specific conductivity values before and after the permeabilization, respectively, and E_0 and E_1 are the reversible and the irreversible electric field thresholds, respectively. Parameter B defines the shape of the exponential and sigmoid functions.

IV. Results

A. The Threshold Values and the Specific Conductivity Changes in Single Tissues

To build a sequential model of electroporation of subcutaneous tumor, we have to know the electropermeabilization threshold values and conductivity changes for all tissues involved. To estimate these values we used data from literature (for skin [18] and [19]) and experimentally collected data (for muscle, skinfold, and tumor), such as current-voltage dependencies and $^{51}\mathrm{Cr}-\mathrm{EDTA}$ uptake.

The electric field threshold values of the reversible and the irreversible electropermeabilization of the skeletal muscle and tumor melanoma and sarcoma were estimated based on $^{51}\mathrm{Cr}-\mathrm{EDTA}$ uptake method and are graphically presented in Fig. 5. We obtained data for all the tissues of our model, except for the connective tissue.

Current-voltage dependences measured at the end of the pulse for all tissues were used to fine tune the sequential model parameters. Current-voltage curves for the tissues included in the study are presented in Fig. 6. On the abscissa the voltage between the electrodes is normalized with the distance between them. In the case of the homogeneous electric field that would also denote the homogeneous electric field magnitude. But in our case the homogeneity of the electric field is deformed near the edge of the electrode, furthermore because of the chemical reactions additional voltage drop occurs at the skin-electrode

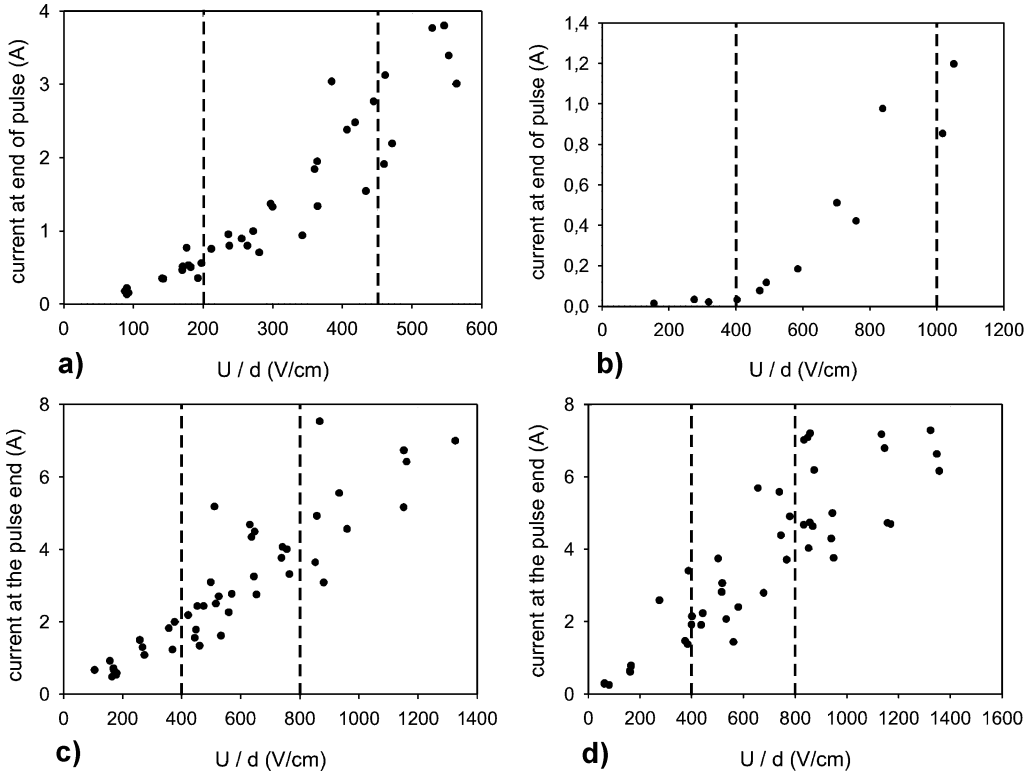

Fig. 6. Current at the end of the pulse with respect to the applied voltage for (a) muscle (electrode distance: 5.7 cm, pulse length: 100 μs). (b) Skinfold (electrode distance: 2.8 cm, pulse length: 100 μs). (c) Tumor melanoma B16 (electrode distance: 5.2 cm, pulse length: 100 μs). and (d) Tumor LPB sarcoma (electrode distance: 5.2 cm, pulse length: 100 μs).

contact. Nevertheless, almost in the entire region between the electrodes where the tissue is, the electric field is almost homogeneous and equals the ratio between the voltage and the distance between the electrodes. Thus the error we make using those electric field values to approximately determine the thresholds of electropermeabilization for the sequential analysis, is small enough. To approximately determine the electroporation thresholds and the specific conductivity changes of the tissues, we used the $^{51}\mathrm{Cr}-\mathrm{EDTA}$ uptake measurements at different pulse voltage amplitudes between the electrodes (Fig. 5). We can also use the current at the end of the pulse at a range of pulse voltage amplitudes (Fig. 6).

The threshold values of the electric field intensity were determined empirically using data on $^{51}\mathrm{Cr}-\mathrm{EDTA}$ uptake and current at the end of the pulse. Thresholds present linear regressions to field intensities corresponding to low uptake values, increasing uptake values, and decreasing uptake values (Fig. 5); as well as linear regressions to field intensities corresponding to slope changes in the current at the end of the pulse measurements (Fig. 6). Threshold values of reversible and irreversible electroporation were determined as the field intensities corresponding to intersections of consecutive linear regressions. They are plotted on Figs. 5 and 6 using dashed vertical lines. We determined the approximate threshold values to be: for the muscle: 200 V/cm (reversible) and 450 V/cm (irreversible), for the skin: 400 V/cm (reversible) and 1000 V/cm (irreversible) and for the tumor: 400 V/cm (reversible) and 800 V/cm (irreversible).

With the sequential analysis we calculated the electric field distribution and the reaction current through the single tissue model at the end of the electroporation process. The reaction currents for different voltages were then compared with the experimental data on graphs in Fig. 6. The electroporation process data [initial specific conductivities, electropermeabilization thresholds, change in specific conductivity and the specific conductivity dependence between the thresholds $(\sigma(\mathrm{E}))$] was then fine tuned so that we found a good agreement between the current measured in experiments and that given by the model.

No experimental data on electroporation of the connective tissue existed. Therefore the electric field thresholds and specific conductivity changes could not be established for that layer. Those parameters were therefore set without any experimental confirmation of the model. Fig. 7 shows the reaction currents of single tissue models compared to the experimental data shown above.

In Table I the electroporation parameters for all the tissues used in the subcutaneous tumor model are presented. We chose the functions describing the specific conductivity dependence on electric field intensity between the reversible and the irreversible thresholds based on criteria that the output of the models should best fit the experimental data. Since we did not have any experimental data on connective tissue, we used the simplest of the functions—the step function. Theoretically, a sigmoid model of the electroporation process seems the most logical one. Namely, due to the nonuniformity of the cell size and shape in the tissue, not all the cells are permeabilized at the same time once E_0 is reached. Furthermore, when the electric field is reaching the irreversible threshold E_1, cell nonuniformity would also lead to a gradual saturation of the

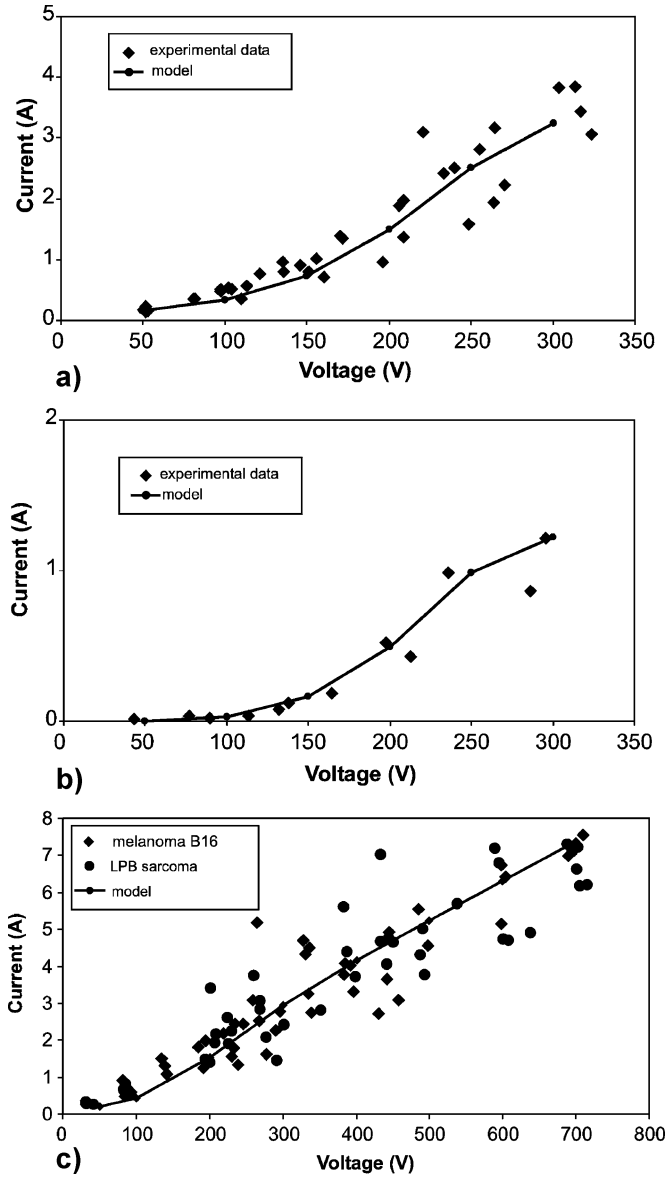

Fig. 7. The comparison of the reaction current vs. applied voltage between the experimental data and the EMAS models of (a) muscle (electrode distance: 5.7 cm, pulse length: 100 μs), (b) skinfold (electrode distance: 2.8 cm, pulse length: 100 μs), and (c) tumor—melanoma B16 and LPB sarcoma together, (electrode distance: 5.2 cm, pulse length: 100 μs).

$\sigma(\mathrm{E})$ curve. We tried all the functions available to describe the $\sigma(\mathrm{E})$ dependences on all the tissues. We noticed that the $\sigma(\mathrm{E})$ behavior of all tissues can be described with practically each of the functions tested, with proper adjustments of other parameters such as the reversible and irreversible thresholds and the increase in the specific conductivity of the tissue. However, the adjustments may be too far from the biologically justifiable values determined from the experiments. So we always chose the function that best presented the $\sigma(\mathrm{E})$ dependence without the need for significant adjustments of other parameters. This empirical approach resulted in choosing electroporation models other than the sigmoid.

The irreversible threshold of skin used in the numerical model was slightly different to the one proposed in Fig. 6 (1000 V/cm), to better fit the *in vivo* measurements. The reversible threshold and the conductivity change of connective tissue were set similar to those of the muscle and the tumor since it seemed that that is the order of magnitude of the conductivity changes in tissues except skin.

B. Intricate Subcutaneous Tumor Model

The electric field threshold values, changes in specific conductivity and the functions describing the conductivity changes due to electroporation for each tissue separately determined in the previous section were used in the subcutaneous tumor model. The electric field distribution was modeled before, during and after the electroporation process.

Sequential analysis was initiated three times with three different voltages between the electrodes: 500, 1000, and 1500 V. In Fig. 8 six steps of the electroporation process in the subcutaneous tumor model for the voltage of 1000 V between the electrodes are shown. The electric field distribution is shown in V/cm. Step 0 denotes the electric field distribution as it was before the electroporation process started, thus when all the tissues had their initial specific conductivities.

When the voltage is applied to the electrodes, the electric field is distributed in the tissue according to specific conductivity ratios of the tissues in the model. The field strength is the highest in the tissues with the lowest specific conductivity, where the voltage drop is the largest and the voltage gradient the highest. In our case, almost the entire voltage drop occurs in the skin layer which has a specific conductivity of about 10–100 times lower than the tissues lying underneath [18], [19], [40]–[49].

If we look at the last step of the sequential analysis, step 5, at 1000 V (Fig. 8) the tumor is entirely permeabilized, in some areas the electric field is also above the irreversible threshold (800 V/cm). Looking at the sequential analysis at 500 and 1500 V (data shown in Fig. 9, only the last step of the sequential analysis), we can establish that the tumor is partially permeabilized already at 500 V (reversible threshold in the tumor is at 400 V/cm). At 1500 V, a large part of the tumor is above the irreversible electric field threshold. Observing all the steps of the electroporation process, we can see that at the beginning the electric field is the highest in the skin layer. Therefore, the first tissue permeabilized is the skin, and only then the electric field "penetrates" to the deeper layers of the model and causes the rest of the tissues being permeabilized as well. We can see that already in the third step almost the final electric field distribution is reached.

V. Discussion

We built a finite element model of a subcutaneous tumor on small animals to study electropermeabilization of tissues involved. The model was composed of skin, connective tissue, tumor and muscle. We studied the electric field distribution and the reaction currents through the model before, during and after the electroporation process in discrete time steps. The tissue specific conductivity increases when permeabilized, so the electric field distribution changes. Therefore, to study the electroporation process, we need data on the initial, prepulse specific conductivities of the tissues in the model, changes of the specific conductivities of the tissues when permeabilized, and the electric field threshold values for reversible and irreversible electropermeabilization for each tissue separately. We collected nu-

TABLE I
PARAMETERS OF THE ELECTROPORATION PROCESSS FOR TISSUES IN THE SUBCUTANEOUS TUMOR MODEL AS OBTAINED FROM MEASUREMENTS AND SINGLE TISSUE MODELING

tissue	σ(E)	initial specific cond. (S/m)	spec. cond. increase	electric field thresholds (V/cm)
muscle	e^x-1 (B=15.000)	0,735 / 0,11	4 x	rev.: 200; irrev.: 450
skin	e^x-1 (B=30.000)	0,002	80 x	rev.: 400; irrev.: 900
tumor	1-e^x (B=15.000)	0,3	2,5 x	rev.: 400; irrev.: 800
connective tiss.	step	0,03	3 x	rev.: 300

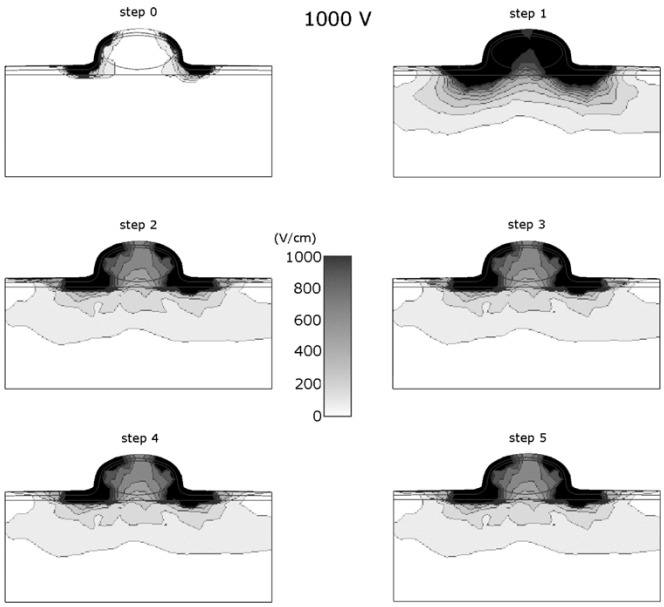

Fig. 8. Six steps of the sequential analysis of the electroporation process in the subcutaneous tumor model at 1000 V between two plate electrodes with distance of 8 mm. Time intervals between steps are in general not uniform. Different steps follow a chronological order but do not have an exact time value associated with them. The electric field distribution is shown in V/cm.

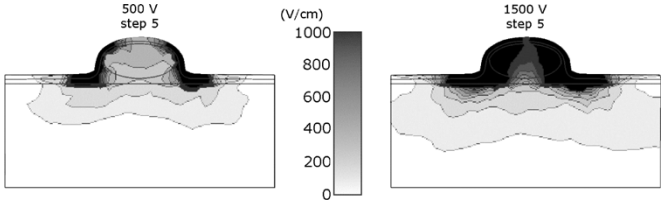

Fig. 9. The last step of the sequential analysis of the electroporation process in the subcutaneous tumor model at 500 and 1500 V, respectively, between two plate electrodes with distance of 8 mm. Time intervals between steps are in general not uniform. Different steps follow a chronological order but do not have an exact time value associated with them. The electric field distribution is shown in V/cm.

merical values of the initial specific conductivity from [18], [19], [26]–[45].

We noticed large discrepancies between the data reported by different researchers. These are due to many factors, such as different measuring techniques used, the fact that tissue samples were taken from different species, circumstances under which the measurements were performed (*in vivo*, *ex vivo*, time elapsed after the death of the animal, tissue temperature...), and others

TABLE II
RANGES OF VALUES FOR SPECIFIC CONDUCTIVITIES FOUND IN THE LITERATURE [18], [19], AND [26]–[45]

		specific conductivity (S/m)
tumor		0.22 0.4
connective tissue		0.02 0.04
muscle	transversal	0.04 0.14
	longitudinal	0.3 0.8
skin (dry)		0.00002 0.0002
skin (wet)		0.0003 0.2
stratum corneum		0.0000125
skin lower layers		0.227

(tissue seasonal changes, the age of the object, possible pathological condition of the object, ...). In Table II we present the low-frequency (all below 100 Hz) value ranges of the tissues in question.

We set the reversible and irreversible electric field threshold values and the conductivity changes of the tissues with the help from $^{51}\mathrm{Cr}-\mathrm{EDTA}$ uptake data and current vs. voltage dependences, comparing the model with experimental data we collected for each tissue separately. Finite element models of the experimental tissue-electrode setups were built for each tissue. In the models, we had to change the specific conductivities during the electroporation process. We developed a computer application which in combination with the commercial software package EMAS, computes the electroporation process in discrete steps.

Not the same function could be used to describe the specific conductivity dependence on the electric field $(\sigma(\mathrm{E}))$ for all the tissues. This is probably due to the biological differences between the tissues (such as cell size and distribution, different electrical properties of the intracellular media, differences in the structural inhomogeneity of the tissues (necrosis in tumors), ion concentration...). We believe those differences are the reason for different propagation of permeabilization in tissues.

We compared our results for skin tissue with data from [18] and [19]. Good agreement was established in both, threshold values and conductivity changes. Namely, in the abovementioned papers a big change in tissue resistivity was observed for voltages above 50 V. It has to be emphasized that in this case the experiments were made through a single skin thickness, while

in our case we have a skinfold which corresponds to a double thickness, thus, 100 V of applied voltage. We indeed observed changes in skin conductivity above 100 V. Also the changes in specific conductivity are in good agreement, namely the values found in the literature state the range of approximately 40 to 2000 times increase of specific conductivity, depending on the applied voltage.

After tuning the current vs. voltage dependences of the single tissue models with the experimental data, we used the electric field threshold values, changes in specific conductivity and the specific conductivity dependences $(\sigma(\mathrm{E}))$ between the reversible and the irreversible electric field in the subcutaneous tumor model. We initiated the sequential analysis three times, with three different voltages between the electrodes: 500, 1000, and 1500 V. Studying the last step for each sequential analysis, we can see that the tumor is partially permeabilized already at 500 V, at 1000 V the tumor is entirely permeabilized and in some areas, the electric field is already above the irreversible threshold, and at 1500 V, almost the entire tumor is above the irreversible threshold.

The model was validated by comparison of the computed electric field distributions with some experimental results of electrochemotherapy [50], [51]. Experimental results for treatments with 8 mm distance between electrodes show antitumor effectiveness of electrochemotherapy with cis-diamminedichloroplatinum(II) (CDDP) for amplitudes exceeding 720 V. Antitumor effect increased at 1200 V, however this or higher amplitudes can result in severe side effects as a result of tumor lysis syndrome, due to massive tumor destruction. Nevertheless, antitumor effects (increased tumor growth delay) can be achieved also at 1040 V, where minimal antitumor effect of electroporation itself is observed and most of the tumor cells are permeabilized. Our model distributions together with the reversible and irreversible electric field thresholds obtained from *in vivo* measurements coincide well with the effectiveness of the electrochemotherapy and the necrosis stage of tumors, depending on the electroporation amplitude.

Thus a preliminary numerical model of subcutaneous tumor in small animals has been made available. Its extension to other geometries would allow forecasting the outcome of pulse delivery before the treatment. Such an approach could optimize the choice of electrodes and their placement in both electrochemotherapy and gene transfer.

REFERENCES

[1] E. Neumann, A. E. Sowers, and C. A. Jordan, *Electroporation and Electrofusion in Cell Biology*. New York: Plenum, 1989.

[2] J. C. Weaver and Y. A. Chizmadzhev, "Theory of electroporation: a review," *Bioelectrochem. Bioenerg.*, vol. 41, pp. 135–160, 1996.

[3] T. Y. Tsong, "Electroporation of cell membranes," *Biophys. J.*, vol. 60, pp. 297–306, 1991.

[4] L. M. Mir, "Therapeutic perspectives of *in vivo* cell electropermeabilization (Review Article)," *Bioelectrochem.*, vol. 53, pp. 1–10, 2000.

[5] D. Miklavčič, D. Šemrov, H. Mekid, and L. M. Mir, "A validated model of *in vivo* electric field distribution in tissues for electrochemotherapy and for DNA electrotransfer for gene therapy," *Biochim. Biophys. Acta*, vol. 1519, pp. 73–83, 2000.

[6] M. Pavlin, N. Pavšelj, and D. Miklavčič, "Dependence of induced transmembrane potential on cell density, arrangement and cell position inside a cell system," *IEEE Trans. Biomed. Eng.*, vol. 49, no. 6, pp. 605–612, Jun. 2002.

[7] B. Valič, M. Golzio, M. Pavlin, A. Schatz, C. Faurie, B. Gabriel, J. Teissié, M. P. Rols, and D. Miklavčič, "Effect of electric field induced transmembrane potential on spheroidal cells: theory and experiment," *Eur. Biophys. J.*, vol. 32, pp. 519–528, 2003.

[8] B. Valič, M. Pavlin, and D. Miklavčič, "The effect of resting transmembrane voltage on cell electropermeabilization: a numerical analysis," *Bioelectrochemistry*, vol. 63, pp. 311–315, 2004.

[9] H. Wolf, M. P. Rols, E. Boldt, E. Neumann, and J. Teissie, "Control by pulse parameters of electric field—mediated gene transfer in mammalian cells," *Biophys. J.*, vol. 66, pp. 524–531, 1994.

[10] D. Miklavčič, K. Beravs, D. Šemrov, M. Čemažar, F. Demšar, and G. Serša, "The importance of electric field distribution for effective *in vivo* electroporation of tissues," *Biophys. J.*, vol. 74, pp. 2152–2158, 1998.

[11] M. Pavlin and D. Miklavčič, "Effective conductivity of a suspension of permeabilized cells: a theoretical analysis," *Biophys. J.*, vol. 85, pp. 719–729, 2003.

[12] R. V. Davalos, B. Rubinsky, and D. M. Otten, "A feasibility study for electrical impedance tomography as a means to monitor tissue electroporation for molecular medicine," *IEEE Trans. Biomed. Eng.*, vol. 49, no. 4, pp. 400–403, Apr. 2002.

[13] D. Šemrov and D. Miklavčič, "Numerical modeling for *in vivo* electroporation," in *Methods in Molecular Medicine*. Totowa, NJ: Humana, 2000, vol. 37, Electrically mediated delivery of molecules to cells.

[14] ——, "Calculation of the electrical parameters in electrochemotherapy of solid tumours in mice," *Comput. Biol. Med.*, vol. 28, pp. 439–448, 1998.

[15] S. Tungjitkusolmun, E. J. Woo, H. Cao, J.-Z. Tsai, V. R. Vorperian, and J. G. Webster, "Thermal-electrical finite element modeling for radio frequency cardiac ablation: effects of changes in myocardial properties," *Med. Biolog. Eng. Comput.*, vol. 38, pp. 562–568, 2000.

[16] P. M. Ghosh, C. R. Keese, and I. Giaever, "Monitoring electropermeabilization in the plasma membrane of adherent mammalian cells," *Biophys. J.*, vol. 64, pp. 1602–1609, 1993.

[17] R. V. Davalos, D. M. Otten, L. M. Mir, and B. Rubinsky, "Electrical impedance tomography for imaging tissue electroporation," *IEEE Trans. Biomed. Eng.*, vol. 51, pp. 761–767, 2004.

[18] U. Pliquett, R. Langer, and J. C. Weaver, "Changes in the passive electrical properties of human stratum corneum due to electroporation," *BBA*, vol. 1239, no. 5, pp. 111–121, May 1995.

[19] U. Pliquett and J. C. Weaver, "Electroporation of human skin: simultaneous measurement of changes in the transport of two fluorescent molecules and in the passive electrical properties," *Bioelectrochem. Bioenerg.*, vol. 39, pp. 1–12, 1996.

[20] U. Pliquett, R. Elez, A. Piiper, and E. Neumann, "Electroporation of subcutaneous mouse tumors by rectangular and trapezium high voltage pulses," *Bioelectrochemistry*, vol. 62, pp. 83–93, 2004.

[21] M. Schmeer, T. Seipp, U. Pliquett, S. Kakorin, and E. Neumann, "Mechanism for the conductivity changes caused by membrane electroporation of CHO cell-pellets," *Phys. Chem. Chem. Phys.*, vol. 6, no. 24, pp. 5564–5574, 2004.

[22] *EMAS User's Manual*, Ansoft Corp., Jul. 1997.

[23] B. Irons and S. Ahmad, *Techniques of Finite Elements*. New York: Wiley, 1986.

[24] R. Susil, D. Šemrov, and D. Miklavčič, "Electric field—induced transmembrane potential depends on cell density and organization," *Electro. Magnetobiol.*, vol. 17, no. 3, pp. 391–399, 1998.

[25] J. Gehl and L. M. Mir, "Determination of optimal parameters for *in vivo* gene transfer by electroporation, using a rapid *in vivo* test for cell permeabilization," *Biochem. Biophys. Res. Commun.*, vol. 261, pp. 377–380, 1999.

[26] L. A. Geddes and L. E. Baker, "The specific resistance of biological material—a compendium of data for the biomedical engineer and physiologist," *Med. Biol. Eng.*, vol. 5, pp. 271–293, 1967.

[27] H. P. Schwan and C. F. Kay, "Specific resistance of body tissues," *Circ. Res.*, vol. 4, pp. 664–670, 1956.

[28] B. R. Epstein and K. R. Foster, "Anisotropy in the dielectric properties of skeletal muscle," *Med. Biol. Eng. Comput.*, vol. 21, no. 1, pp. 51–55, 1983.

[29] H. C. Burger and R. Van Dongen, "Specific resistance of body tissues," *Phys. Med. Biol.*, vol. 5, pp. 431–447, 1960.

[30] S. Rush, J. A. Abildskov, and R. McFee, "Resistivity of body tissues at low frequencies," *Circ. Res.*, vol. 12, pp. 40–50, 1963.

[31] F. X. Hart, "The impedance spectroscopy of skeletal muscle," in *10th Electrotech. Comput. Science Conf. ERK 2001*, vol. A, 2001, pp. 13–16.

[32] C. Gabriel, S. Gabriel, and E. Corthout, "The dielectric properties of biological tissue: i. literature survey," *Phys. Med. Biol.*, vol. 41, pp. 2231–2249, 1996.

[33] S. Gabriel, R. W. Lau, and C. Gabriel, "The dielectric properties of biological tissue: ii. measurements in the frequency range 10 Hz to 20 GHz," *Phys. Med. Biol.*, vol. 41, pp. 2251–2269, 1996.
[34] ——, "The dielectric properties of biological tissue: iii. parametric models for the dielectric spectrum of tissues," *Phys. Med. Biol.*, vol. 41, pp. 2271–2293, 1996.
[35] S. R. Smith, K. R. Foster, and J. L. Wolf, "Dielectric properties of VX-2 carcinoma vs. normal liver tissues," *IEEE Trans. Biomed. Eng.*, vol. BME-33, no. 5, pp. 522–524, May 1986.
[36] A. J. Surowiec, S. S. Stuchly, J. R. Barr, and A. Swarup, "Dielectric properties of breast carcinoma and the surrounding tissues," *IEEE Trans. Biomed. Eng.*, vol. 35, no. 4, pp. 257–263, Apr. 1988.
[37] H. P. Schwan and C. F. Kay, "The conductivity of living tissues," *Ann. NY Acad. Sci.*, vol. 65, pp. 1007–1013, 1957.
[38] F. L. H. Gielen, W. Wallinga-de Jonge, and K. L. Boon, "Electrical conductivity of skeletal muscle tissue: experimental results from different muscles *in vivo*," *Med. Biolog. Eng.*, vol. 22, pp. 569–577, 1984.
[39] B. Bodakian and F. X. Hart, "The dielectric properties of meat," *IEEE Trans. Dielect. Elect. Insul.*, vol. 1, no. 2, pp. 181–187, Apr. 1994.
[40] W. Kaufman and F. D. Johnston, "The electrical conductivity of the tissues near the heart and its bearing on the distribution of cardiac action currents," *Am. Heart J.*, vol. 26, pp. 42–54, 1943.
[41] A. Hemingway and J. F. McLendon, "The high frequency resistance of human tissue," *Am. J. Physiol.*, vol. 102, pp. 56–59, 1932.
[42] H. P. Schwan and K. Li, "Capacity and conductivity of body tissues at ultrahigh frequencies," in *Proc. IRE*, vol. 41, 1953, pp. 1735–1740.
[43] E. Kinnen, W. Kubicek, P. Hill, and G. Turton, "Thoracic Cage Impedance Measurements. (Tissue Resistivity *in vivo* and Transthoracic Impedance at 100 kc/s)," School of Aerospace Medicine, Brooks AFB, TX, Tech. Doc. Rep. SAM-TDR 64-5, 1964.
[44] T. Yamamoto and Y. Yamamoto, "Electrical properties of the epidermal stratum corneum," *Med. Biol. Eng.*, vol. 14, no. 2, pp. 151–158, 1976.
[45] ——, "Dielectric constant and resistivity of epidermal stratum corneum," *Med. Biol. Eng.*, vol. 14, no. 5, pp. 494–500, 1976.
[46] U. Pliquett, "Mechanistic studies of molecular transdermal transport due to skin electroporation," *Adv. Drug Deliv. Rev.*, vol. 35, pp. 41–60, 1999.
[47] M. R. Prausnitz, V. G. Bose, R. Langer, and J. C. Weaver, "Electroporation of mammalian skin: a mechanism to enhance transdermal drug delivery," *Proc. Nat. Acad. Sci. USA*, vol. 90, pp. 10 504–10 508, 1993.
[48] Y. A. Chizmadzhev, A. V. Indenbom, P. I. Kuzmin, S. V. Galichenko, J. C. Weaver, and R. O. Potts, "Electrical properties of skin at moderate voltages: contribution of appendageal macropores," *Biophys. J.*, vol. 74, pp. 843–856, 1998.
[49] S. A. Gallo, A. R. Oseroff, P. G. Johnson, and S. W. Hui, "Characterization of electric-pulse-induced permeabilization of porcine skin using surface electrodes," *Biophys. J.*, vol. 72, pp. 2805–2811, 1997.
[50] G. Serša, M. Čemažar, and D. Miklavčič, "Anti-tumor efectiveness of electrochemotherapy with cis-Diamminedichloroplatinum(II) in mice," *Cancer Res.*, vol. 55, pp. 3450–3455, 1995.
[51] G. Serša, M. Čemažar, D. Miklavčič, and D. J. Chaplin, "Tumor blood flow modifying effect of electrochemotherapy with bleomycin," *Anticancer Res.*, vol. 19, pp. 4017–4022, 1999.

Nataša Pavšelj was born in 1974 in Ljubljana, Slovenia. She received the B.Sc. and M.Sc. degree in electrical engineering from the Faculty of Electrical Engineering, University of Ljubljana. She is currently working toward the Ph.D. degree at the University of Ljubljana.

Her main research interests lie in the field of electroporation, including numerical modeling of electric field distribution in different biological tissue setups and cell systems and comparison of the theoretical results with the experimental work.

Zvonko Bregar was born in 1964 in Kamanje, Croatia. In 1988, he received the B.Sc. degree in application mathematics and the M.Sc. degree in 2000 in computer science from the University of Ljubljana, Ljubljana, Slovenia.

He is with Milan Vidmar Electroinstitute, Ljubljana. His interests lie in various forms of computer modeling and simulations of electric systems.

David Cukjati was born in 1970 in Ljubljana, Slovenia. He received the M.Sc. and Ph.D. degrees in electrical engineering from the University of Ljubljana.

He is currently a Teaching Assistant with the Faculty of Electrical Engineering, University of Ljubljana. He works in the field of biomedical engineering. His current research interests are electrical soft tissue healing and electroporation-assisted drug delivery involving modeling, expert systems, biomedical database, and web applications design.

Danute Batiuskaite was born in 1971. She received the Ph.D. degree in biophysics from the Vytautas Magnus University of Kaunas, Kaunas, Lithuania.

Currently she is a lecturer with the Vytautas Magnus University of Kaunas. Her main research interest is in the field of electroporation of cells and tissues, the search for the optimal electrochemoterapy conditions.

Lluis M. Mir was born in 1954 in Barcelona, Spain. He received the B.Sc. degree from the University of Paris VI, Paris, France, in 1976, and the Ph.D. degree from the University of Toulouse, Toulouse, France, in 1983.

He is a Fellow with the Ecole Normale Supérieure de Paris, France. He is currently Director of Research of the CNRS at the UMR 8121 CNRS-Institute Gustave-Roussy, Villejuif, France. His main interests lie in the fields of membrane electropermeabilization *in vitro* and *in vivo*, especially with regard to the transfer of antitumor drugs after tumor cells electroporation (electrochemotherapy) and to the electrotransfer of genes (electrogenetherapy) to healthy and malignant tissues. He is also Professor Adjunct, and since December 2004, Honorary Senator, of the University of Ljubljana, Slovenia.

Damijan Miklavčič was born in 1963 in Ljubljana, Slovenia. He received the Ph.D. degree in electrical engineering from the University of Ljubljana.

He is a Professor with the Faculty of Electrical Engineering, University of Ljubljana, and the Head of Laboratory of Biocybernetics. He is active in the field of biomedical engineering. His current interest focuses on electroporation-assisted drug delivery, including cancer treatment by means of electrochemotherapy, tissue oxygenation, and modeling.